Electronic Supplementary Material (ESI) for Inorganic Chemistry Frontiers.
This journal is © the Partner Organisations 2017

Supporting Information

Complementation and Joint Contribution of Appropriate Intramolecular Coupling and Local Ion Symmetry to Improve Magnetic Relaxation in Series of Dinuclear Dy2 Single-Molecule Magnets

Hao-Ran Tu,[†] Wen-Bin Sun,[†] Hong-Feng Li,[†] Peng Chen,[†] Yong-Mei Tian,*[†] Wan-Ying Zhang,[†] Yi-Quan Zhang,*[‡] and Peng-Fei Yan[†]*

[†]Department Key Laboratory of Functional Inorganic Material Chemistry Ministry of Education, Heilongjiang University, Harbin 150080, China.

[‡]Jiangsu Key Laboratory for NSLSCS, School of Physical Science and Technology, Nanjing Normal University, Nanjing 210023, China.

E-mail：wenbinsun@126.com; zhangyiquan@njnu.edu.cn

Table S1. Crystallographic parameters of all complexes.

	1	***2***	***3***	***3Y***
formula	$C_{72}H_{50}Dy_2F_{12}O_{14}$	$C_{56}H_{42}Dy_2F_{12}O_{14}$	$C_{48}H_{38}Dy_2F_{12}O_{14}S_4$	$C_{48}H_{38}Y_2F_{12}O_{14}S_4$
FW ($g.mol^{-1}$)	1692.12	1491.90	1520.02	1372.84
Crystal system	monoclinic	triclinic	triclinic	triclinic
Space group	C1	P-1	P-1	P-1
Temperature (K)	293(2)	293(2) K	293(2) K	293(2)
a (Å)	26.2297(6)	9.7688(6)	10.9116(4)	10.9144(7)
b (Å)	14.2596(3)	12.7894(8)	11.0698(5)	11.0520(9)
c (Å)	18.5801(5)	13.0685(8)	13.0230(5)	13.0251(12)
α (°)	90	113.112(6)	71.207(4)	71.071(8)
β (°)	105.255(3)	105.241(5)	76.793(3)	76.611(7)
γ (°)	90	99.434(5)	67.239(4)	67.152(7)
V ($Å^3$)	6704.6(3)	1381.69(14)	1363.46(9)	1359.50(19)
ρcacd ($Mg.m^{-3}$)	1.676	1.793	1.851	1.677
μ (mm^{-1})	2.311	2.790	2.976	2.382
F (000)	3336	730	742	688
Collected reflections	17704	11173	10673	10797
Independent relections	8606	6347	6167	6189
Rint	0.0248	0.0676	0.0307	0.0320
R1 [$I > 2\sigma(I)$]	0.0869	0.0699	0.0504	0.0946
wR^2 (all data)	0.1672	0.1627	0.1182	0.1913
GOF	1.059	1.088	1.095	1.035

1a	***4***	***4a***	***5***	***6***
$C_{74}H_{62}Dy_2F_{12}O_{18}$	$C_{72}H_{50}F_{12}O_{14}Tb_2$	$C_{74}H_{58}F_{12}O_{18}Tb_2$	$C_{72}H_{50}Er_2F_{12}O_{14}$	$C_{74}H_{58}F_{12}Gd_2O_{18}$
1792.24	1684.96	1781.04	1701.64	1777.70
Triclinic	Monoclinic	Triclinic	Monoclinic	Triclinic
P 1	C2/c	P-1	C2/c	P-1
293(2)	293(2)	293(2)	293(2)	293(2)
10.4693(5)	26.2874(7)	10.4870(5)	26.1533(5)	10.5094(9)
14.2053(8)	14.2711(4)	14.2174(7)	14.2224(3)	14.2002(10)
14.5234(7)	18.5381(6)	14.5235(7)	18.6514(5)	14.5239(11)
105.513(5)	90.00	65.286(4)	90.00	65.464(7)
101.950(4)	105.300(3)	78.174(4)	105.158(2)	78.393(7)
111.582(5)	90.00	68.383(4)	90.00	68.374(7)
1819.40(16)	6708.1(3)	1825.41(15)	6696.3(3)	1830.0(2)
1.636	1.668	1.620	1.688	1.613
890	3328.0	884.0	3352.0	882.0
15001	26117	13362	17264	15821
8220	7929	7443	8364	9161
0.0579	0.0717	0.0447	0.0708	0.0525
0.1325	0.1207	0.1130	0.1054	0.1237
1.079	1.052	1.115	0.973	1.051

	7
formula	$C_{48}H_{38}F_{12}Gd_2O_{14}S_4$
FW ($g.mol^{-1}$)	1509.58
Crystal system	triclinic
Space group	P-1
Temperature (K)	293
a (Å)	10.9212(6)

b (Å)	11.0906(6)
c (Å)	13.0365(5)
α (°)	71.247(4)
β (°)	76.901(4)
γ (°)	67.048(5)
V ($Å^3$)	1367.49(13)
ρcacd ($Mg.m^{-3}$)	1.8329
μ (mm^{-1})	2.653
F (000)	739.2
Collected reflections	11433
Independent relections	6742
Rint	0.0375
R1 [I > 2σ(I)]	0.0491
wR^2 (all data)	0.1391
GOF	1.067

Table S2. Selected bond lengths (Å) and Angles (°) for **1**

Dy1-O3	2.283(3)	Dy1-O5	2.300(4)
Dy1-O3’	2.301(3)	Dy1-O6	2.301(4)
Dy1-O4	2.317(4)	Dy1-O7	2.329(4)
Dy1-O2	2.602(4)	Dy1-O1	2.624(4)

O3-Dy(1)-O5	142.73(14)	O3-Dy1-O3’	66.59(14)
O5-Dy1-O3’	138.26(14)	O3-Dy1-O6	88.70(15)
O5-Dy1-O6	87.13(16)	O3’-Dy1-O6	130.42(15)
O3-Dy1-O4	83.58(14)	O5-Dy1-O4	74.46(14)
O3’-Dy1-O4	84.78(13)	O6-Dy1-O4	136.55(15)
O3-Dy1-O7	117.20(15)	O5-Dy1-O7	96.33(15)
O3’-Dy1-O7	82.59(14)	O6-Dy1-O7	71.28(15)
O4-Dy1-O7	148.24(15)	O3-Dy1-O2	129.66(12)
O5-Dy1-O2	76.37(14)	O3’-Dy1-O2	64.60(12)
O6-Dy1-O2	133.30(15)	O4-Dy1-O2	80.58(14)
O7-Dy1-O2	67.67(14)	O3-Dy1-O1	65.20(12)
O5-Dy1-O1	79.38(14)	O3’-Dy1-O1	128.12(12)
O6-Dy1-O1	65.97(15)	O4-Dy1-O1	72.04(14)

Table S3. Selected bond lengths (Å) and Angles (°) for **1a**

Dy1-O3	2.678(4)	Dy1-O7	2.350(4)
Dy1-O4	2.325(4)	Dy1-O6	2.415(5)

Dy1-O5	2.357(4)	Dy1-O2’	2.384(3)
Dy1-O2	2.303(3)	Dy1-O1’	2.563(4)
Dy1-O8	2.435(4)		
O1’-Dy1-O3	144.57(14)	O2-Dy1-O1’	129.31(12)
O2’-Dy1-O1’	64.22(12)	O2-Dy1-O2’	65.72(13)
O2’-Dy1-O3	121.68(12)	O2-Dy1-O3	63.70(12)
O2-Dy1-O4	82.45(13)	O2-Dy1-O5	146.71(13)
O2’-Dy1-O6	73.44(13)	O2-Dy1-O6	82.34(12)
O2-Dy1-O7	132.86(13)	O2’-Dy1-O8	68.61(14)
O2-Dy1-O8	82.42(13)	O4-Dy1-O1’	140.88(14)
O4-Dy1-O2’	133.28(15)	O4-Dy1-O3	64.39(15)
O4-Dy1-O5	71.44(15)	O4-Dy1-O6	137.16(15)
O4-Dy1-O7	92.24(16)	O4-Dy1-O8	74.27(17)
O5-Dy1-O1’	75.28(17)	O5-Dy1-O2’	119.25(14)
O5-Dy1-O3	118.87(14)	O5-Dy1-O6	130.92(13)
O5-Dy1-O8	78.61(15)	O5-Dy1-O8	71.06(15)

O6-Dy1-O1’	76.59(14)	O6-Dy1-O3	72.95(14)
O6-Dy1-O8	142.05(15)	O7-Dy1-O1’	81.25(14)
O7-Dy1-O1’	81.25(14)	O7-Dy1-O2’	134.47(14)
O7-Dy1-O3	71.79(14)	O7-Dy1-O5	69.95(15)
O7-Dy1-O6	70.22(14)	O7-Dy1-O8	140.99(14)
O7-Dy1-O6	128.59(15)		

Table S4. Selected bond lengths (Å) and Angles (°) for **2**

Dy1-O3	2.267(4)	Dy1-O7	2.302(4)
Dy1-O4	2.311(5)	Dy1-O6	2.315(5)
Dy1-O5	2.321(5)	Dy1-O3’	2.324(4)
Dy1-O2	2.597(4)	Dy1-O1	2.627(4)
O3-Dy1-O7	142.30(15)	O3-Dy1-O4	93.19(17)
O7-Dy1-O4	79.65(18)	O3-Dy1-O6	90.09(16)
O7-Dy1-O6	73.52(16)	O4-Dy1-O6	139.56(17)
O3-Dy1-O5	107.64(18)	O7-Dy1-O5	104.96(18)
O4-Dy1-O5	71.43(16)	O6-Dy1-O5	144.57(17)

O3-Dy1-O3’	67.91(16)	O7-Dy1-O3’	139.08(15)
O4-Dy1-O3’	135.89(17)	O6-Dy1-O3’	82.11(15)
O5-Dy1-O3’	76.95(16)	O3-Dy1-O2	131.30(14)
O7-Dy1-O2	77.87(15)	O4-Dy1-O2	127.80(18)
O6-Dy1-O2	133.30(15)	O4-Dy1-O2	80.58(14)
O7-Dy1-O2	75.28(17)	O5-Dy1-O2	69.96(17)
O3’-Dy1-O2	64.23(14)	O3-Dy1-O1	64.48(14)
O7-Dy1-O1	78.61(15)	O4-Dy1-O1	68.66(17)

Table S5. Selected bond lengths (Å) and Angles (°) for **3**

Dy1-O3	2.316(4)	Dy1-O7	2.295(5)
Dy1-O4	2.317(4)	Dy1-O6	2.322(4)
Dy1-O5	2.330(4)	Dy1-O3’	2.261(4)
Dy1-O2	2.583(5)	Dy1-O1	2.594(4)
O3’-Dy1-O7	142.22(18)	O3’-Dy1-O3	67.27(15)
O7-Dy1-O3	137.01(17)	O3’-Dy1-O4	95.88(16)

O7-Dy1-O4	80.33(18)	O3-Dy1-O4	137.28(16)
O3'-Dy1-O6	87.95(15)	O7-Dy1-O6	73.24(17)
O3-Dy1-O6	80.09(14)	O4-Dy1-O6	140.56(16)
O3'-Dy1-O5	106.71(17)	O7-Dy1-O5	107.3(2)
O3-Dy1-O5	76.87(16)	O4-Dy1-O5	70.88(16)
O6-Dy1-O5	144.93(16)	O3'-Dy1-O2	132.31(15)
O7-Dy1-O2	76.48(19)	O3-Dy1-O2	65.43(16)
O6-Dy1-O2	78.45(18)	O5-Dy1-O2	68.06(18)
O7-Dy1-O1	79.07(18)	O3'-Dy1-O1	65.43(16)
O4-Dy1-O2	123.25(17)	O6-Dy1-O1	78.45(18)
O3-Dy1-O1	127.92(14)	O4-Dy1-O1	67.89(15)

Table S6. Continuous Shape Measures (CShMs) of the coordination geometry for Dy(III) ion in complexes **1**, **1a**, **2** and **3** (S values calculated with the Shape program). The *S* values indicated the proximity to the ideal polyhedron, thus, $S = 0$ corresponds to the non-distorted polyhedron. Three closer ideal geometries to the real complex are listed and below is the symmetry and description for each polyhedron.

	1	**1a**	**2**	**3**
JBTPR-8	16.990		3.305	
TT-8	14.686			14.070
BTPR-8	14.909		3.103	16.360
JSD-8			4.955	

JGBF-8		13.780
TCTPR-9	1.164	
CSAPR-9	1.300	
MFF-9	1.704	

JBTPR-8	C2v	Biaugmented trigonal prism J50
TT-8	D2d	Triangular dodecahedron
BTPR-8	C2v	Biaugmented trigonal prism
JSD-8	D2d	Snub diphenoid J84
JGBF-8	D2d	Johnson gyrobifastigium J26
TCTPR-9	D3h	Spherical tricapped trigonal prism
CSAPR-9	C4v	Spherical capped square antiprism
MFF-9	Cs	Muffin

Table S7. Parameters used to fit the Arrhenius plots from Fig. 4 using approximations $1/\tau = 1/\tau_{QTM} + CT^n + \tau_0^{-1}\exp(-U_{eff}/\kappa T)$ (1):

Zero dc field	***1***	***1a***	***2***	**3**
τ_{QTM}^{-1}/s^{-1}	0.0065	0.19	0.13	0.031
$C/s^{-1}k^{-n}$	3.59	0.037	0.0076	0.16
n	3.54	4.58	5.59	3.75
τ_0/s	6.7×10^{-7}	5.02×10^{-7}	2.75×10^{-10}	1.9×10^{-8}
U/k	18.1	70.3	126.3	109.5

$1/\tau = CT^n + \tau_0^{-1}\exp(-U_{eff}/k_BT)$ (2):

Optimum field	***1***	***1a***	***2***	**3**
$C/s^{-1}k^{-n}$	5.70	0.025	0.0077	0.034
n	3.04	4.92	5.63	4.54

τ_0/s	6.97×10^{-6}	1.16×10^{-7}	1.55×10^{-10}	4.6×10^{-9}
U/k	26.9	88.1	131.7	125.7

Table S8. Best fitted parameters (χ_T, χ_S, τ and α) with the extended Debye model for complex **3** under 0 Oe dc field in the temperature range 2-11 K.

T/ K	χ_S / cm^3 mol^{-1}	χ_T / cm^3 mol^{-1}	τ/s	α	R
2	-0.03312	5.05899	0.03097	0.30000	4.9E-004
2.5	-0.03485	4.94485	0.02779	0.30000	4.7E-004
3	-0.01981	4.71217	0.02499	0.29993	4.5E-004
3.5	-0.04103	4.44415	0.02142	0.30000	3.5E-004
4	-0.05068	4.20219	0.01823	0.29993	2.9E-004
4.5	-0.05454	3.95570	0.01474	0.29365	2.8E-004
5	0.06124	3.72771	0.01166	0.28634	3.0E-004
5.5	-0.07120	3.55050	0.00928	0.28478	3.3E-004
6	-0.05677	3.31692	0.00700	0.26282	3.3E-004
6.5	-0.06532	3.16076	0.00550	0.26218	3.0E-004
7	-0.06745	2.98682	0.00419	0.25571	2.8E-004
7.5	-0.06306	2.84395	0.00321	0.25547	2.5E-004
8	-0.07713	2.70754	0.00241	0.26301	2.1E-004
8.5	-0.07558	2.58002	0.00177	0.27579	1.7E-004
9	-0.08103	2.47702	0.00128	0.29725	1.7E-004
9.5	-0.01583	2.35995	0.00091	0.30000	1.8E-004
10	0.05256	2.25143	0.00065	0.29984	2.1E-004
10.5	0.10776	2.15004	0.00044	0.29875	2.6E-004
11	0.24814	2.06991	0.00033	0.30000	2.4E-004
11.5	0.39647	1.99332	0.00026	0.29931	1.9E-0.004

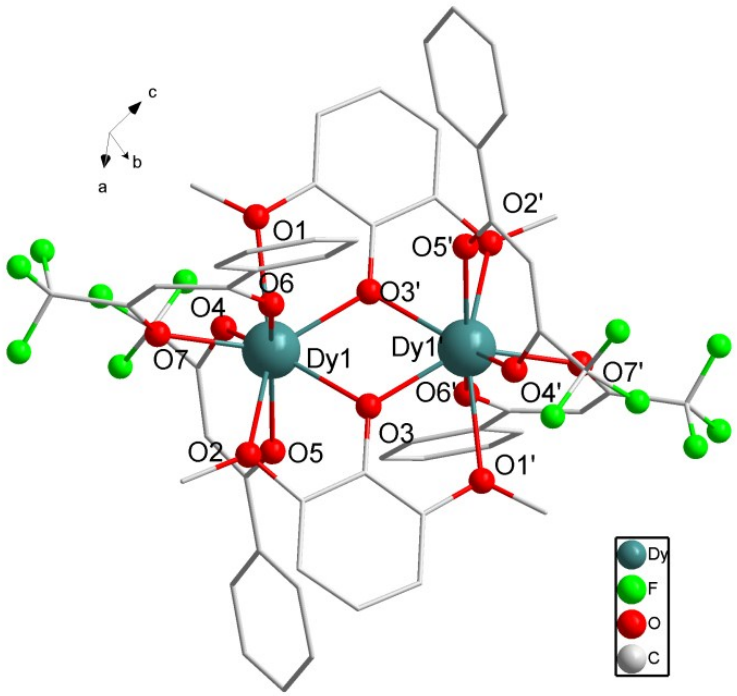

Fig. S1. Molecular structure of complex **2** Colour code: Dy (teal), O (red), F (green), C (grey). H atoms and disorder atoms were omitted for clarity.

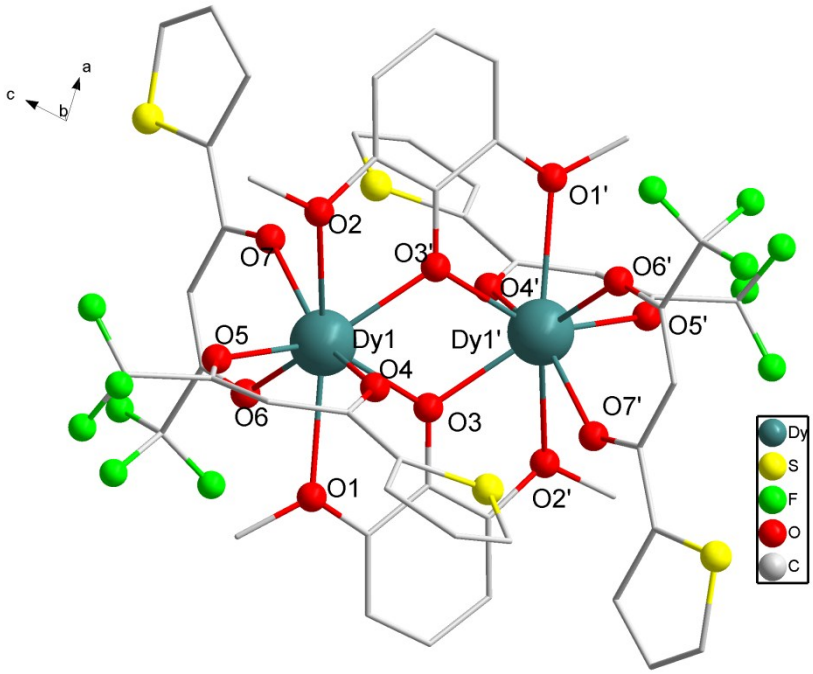

Fig. S2. Molecular structure of complex **3**. Colour code: Dy (teal), O (red), F (green), C (grey), S (yellow). H atoms and disorder atoms were omitted for clarity.

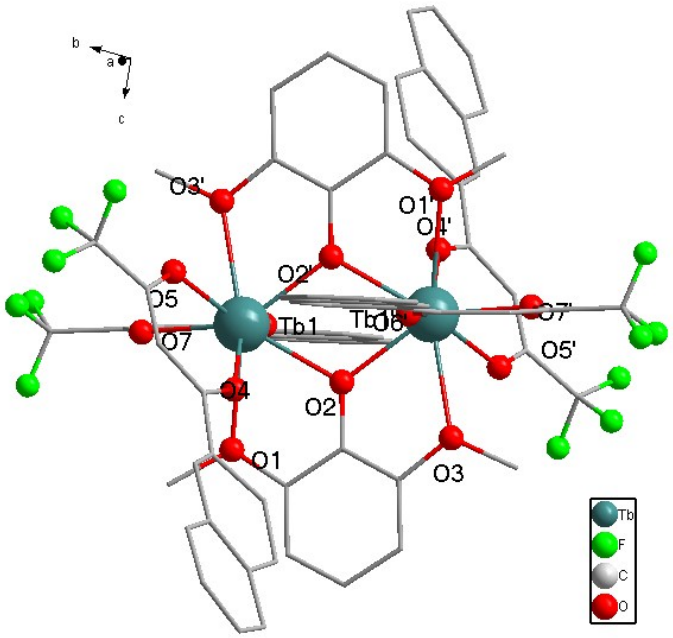

Fig. S3. Molecular structure of complex **4**. Colour code: Tb (teal), O (red), F (green), C (grey). H atoms and disorder atoms were omitted for clarity.

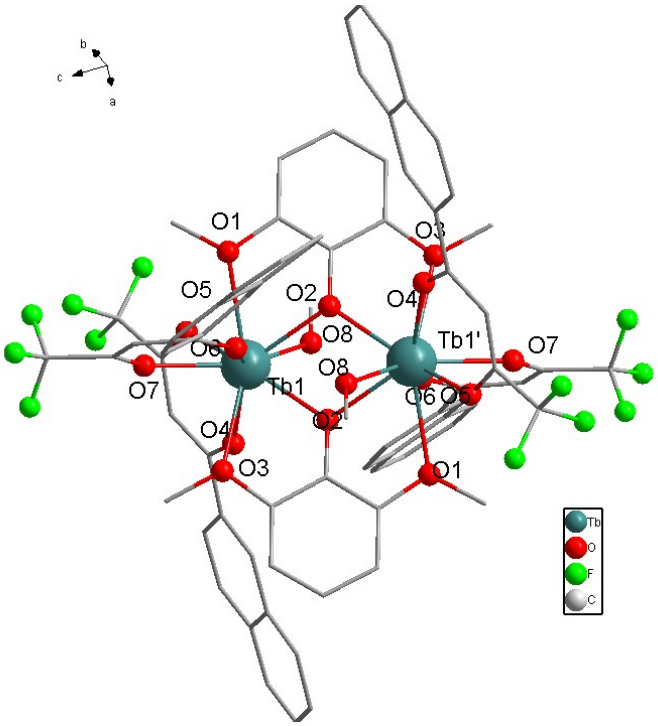

Fig. S4. Molecular structure of complex **4a**. Colour code: Tb (teal), O (red), F (green), C (grey). H atoms and disorder atoms were omitted for clarity.

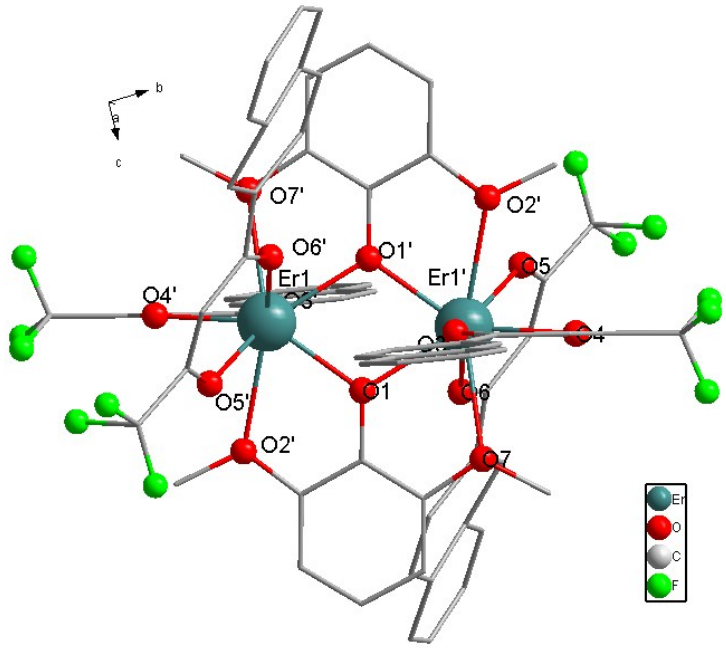

Fig. S5. Molecular structure of complex **5**. Colour code: Er (teal), O (red), F (green), C (grey). H atoms and disorder atoms were omitted for clarity.

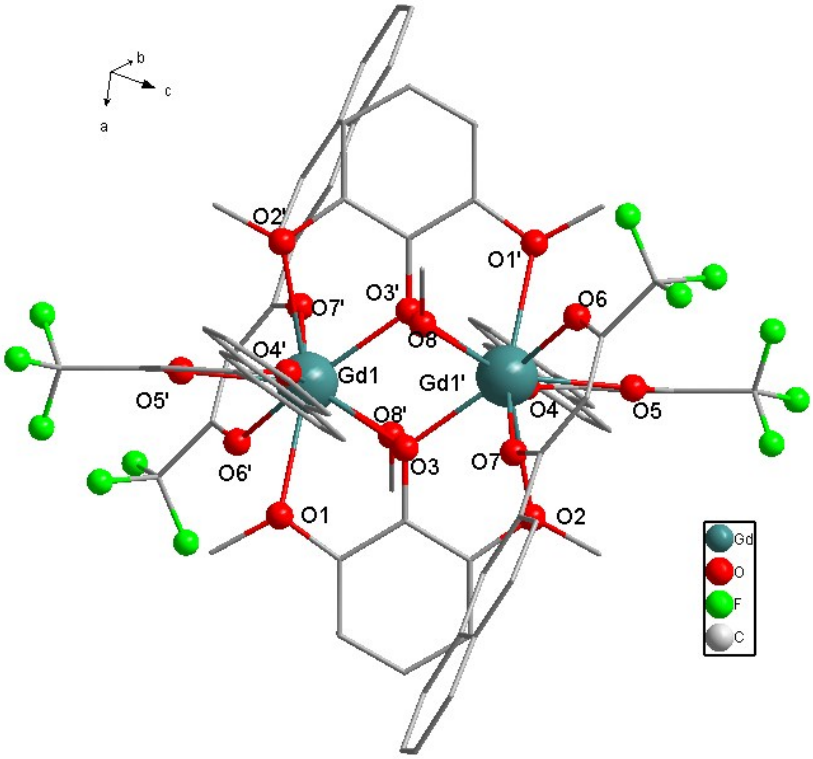

Fig. S6. Molecular structure of complex **6** Colour code: Gd (teal), O (red), F (green), C (grey). H atoms and disorder atoms were omitted for clarity.

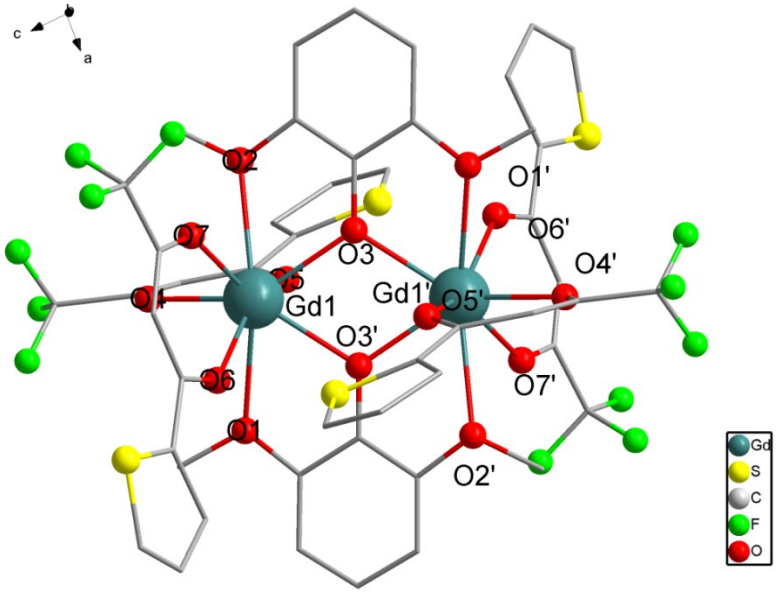

Fig. S7. Molecular structure of **7**. Colour code: Gd (teal), O (red), F (green), S (yellow), C (grey). H atoms and disorder atoms were omitted for clarity.

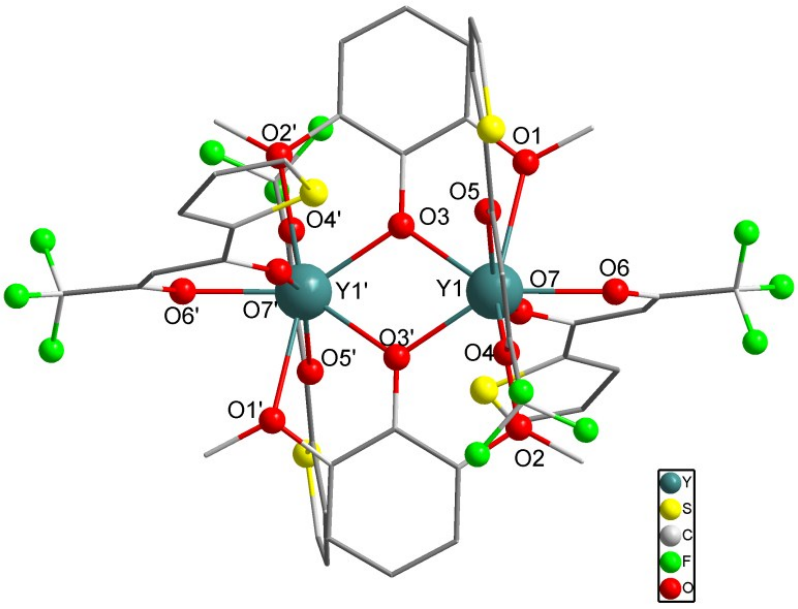

Fig. S8. Molecular structure of **3Y**. Colour code: Dy (teal), O (red), F (green), S (yellow), C (grey). H atoms and disorder atoms were omitted for clarity.

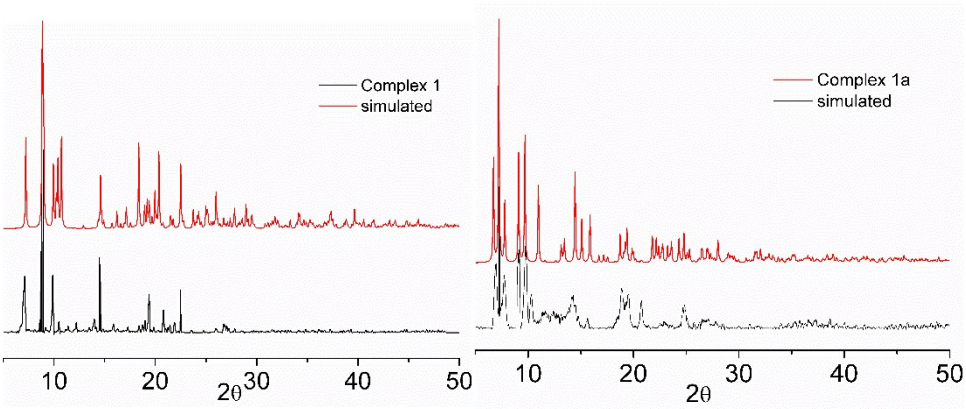
Complex 1
simulated
10
20
30
40
50
2θ

Complex 1a
simulated
10
20
30
40
50
2θ

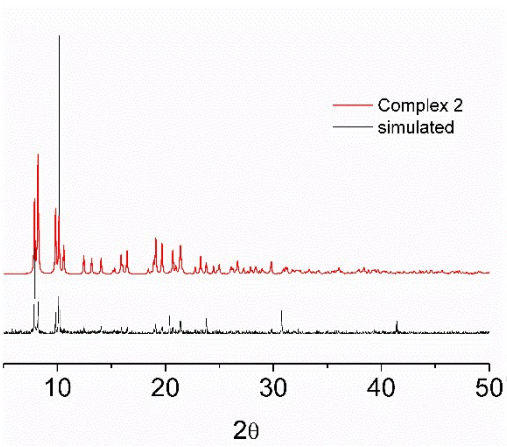
Complex 2
simulated
10
20
30
40
50
2θ

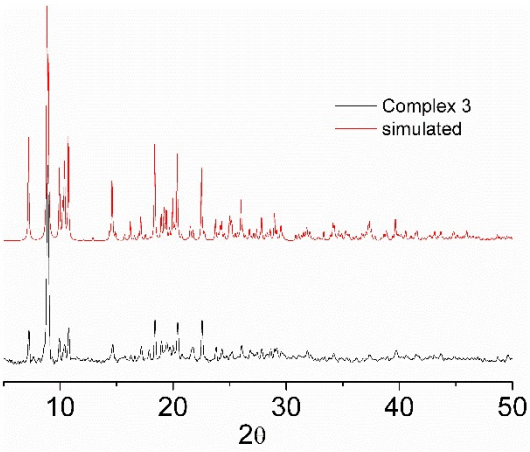
Complex 3
simulated
10
20
30
40
50
2θ

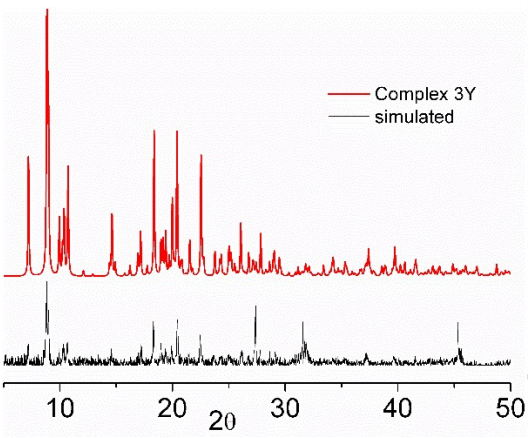
Complex 3Y
simulated
10
20
30
40
50
2θ

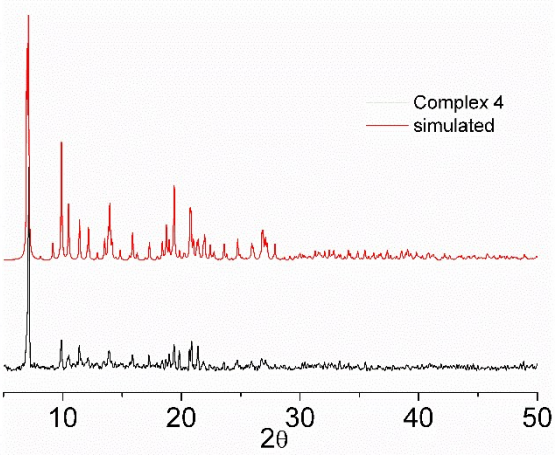
Complex 4
simulated
10
20
30
40
50
2θ

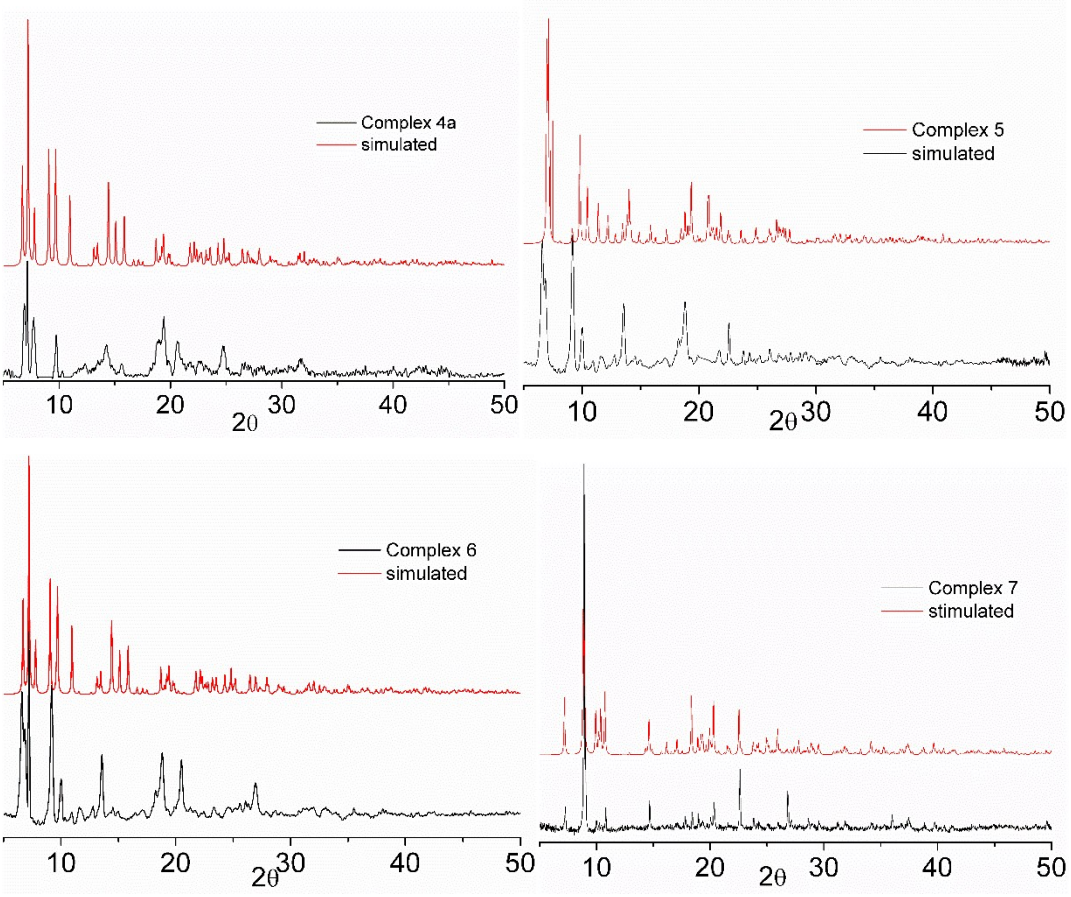

Fig. S9. PXRD analysis of complex **1-7**. The red line is simulated data from single crystal data.

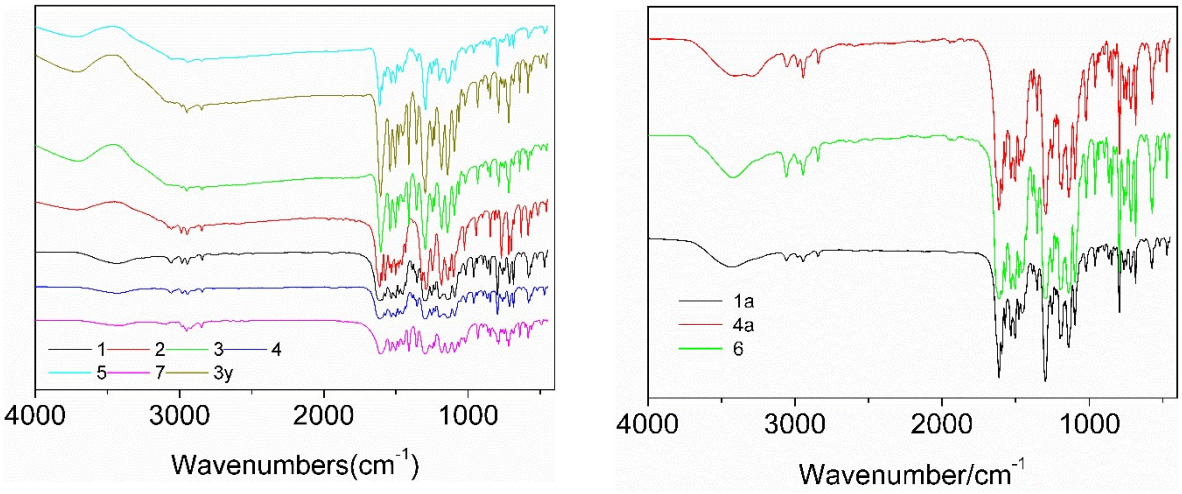

Fig. S10. FT-IR spectra of all the complexes.

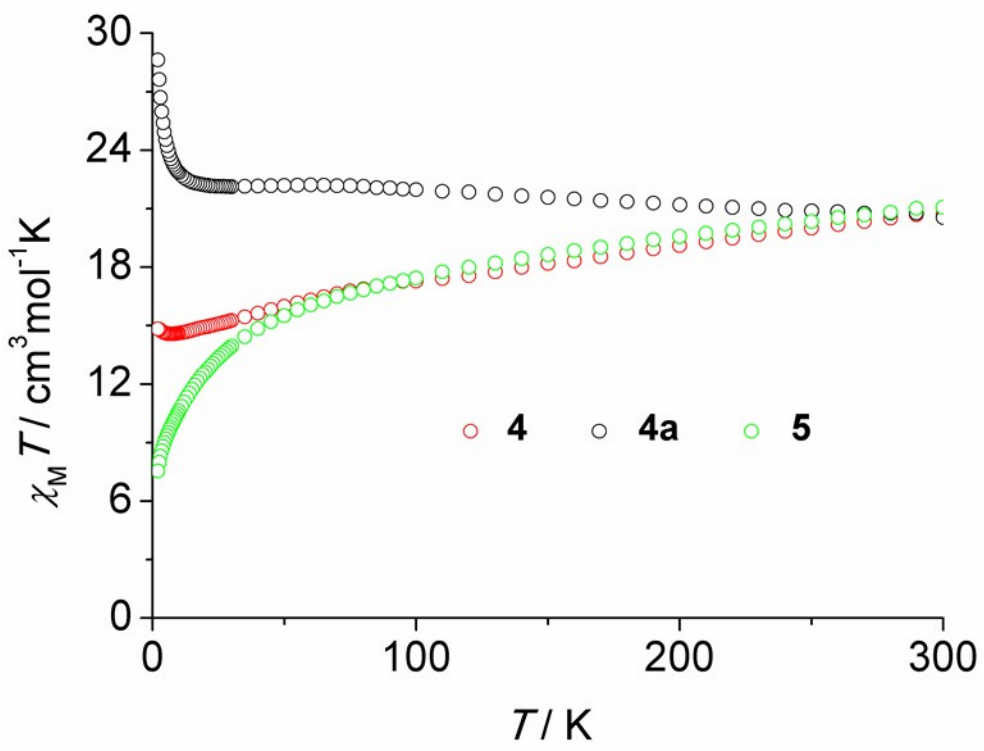

Fig. S11. Temperature dependence of the $\chi_M T$ values T measured for **4**, **4a**, **5** complexes under 1000 Oe dc field.

With the known isotropic interaction, the Hamiltonian H = $-JS_{Gd1} \cdot S_{Gd2}$ results in the formula for the temperature dependence of the molar magnetic susceptibility in eqn (S1), where g is the Landé factor, β is the Bohr magneton, N is the Avogadro number, and k is the Boltzmann constant and $x = -J/k$T.

$$\chi_m T = \frac{2Ng^2\mu_B^2}{k} \frac{e^x + 5e^{3x} + 14e^{6x} + 30e^{10x} + 55e^{15x} + 91e^{21}}{1 + 3e^x + 5e^{3x} + 7e^{6x} + 9e^{10x} + 11e^{15x} + 13e}$$

(S1)

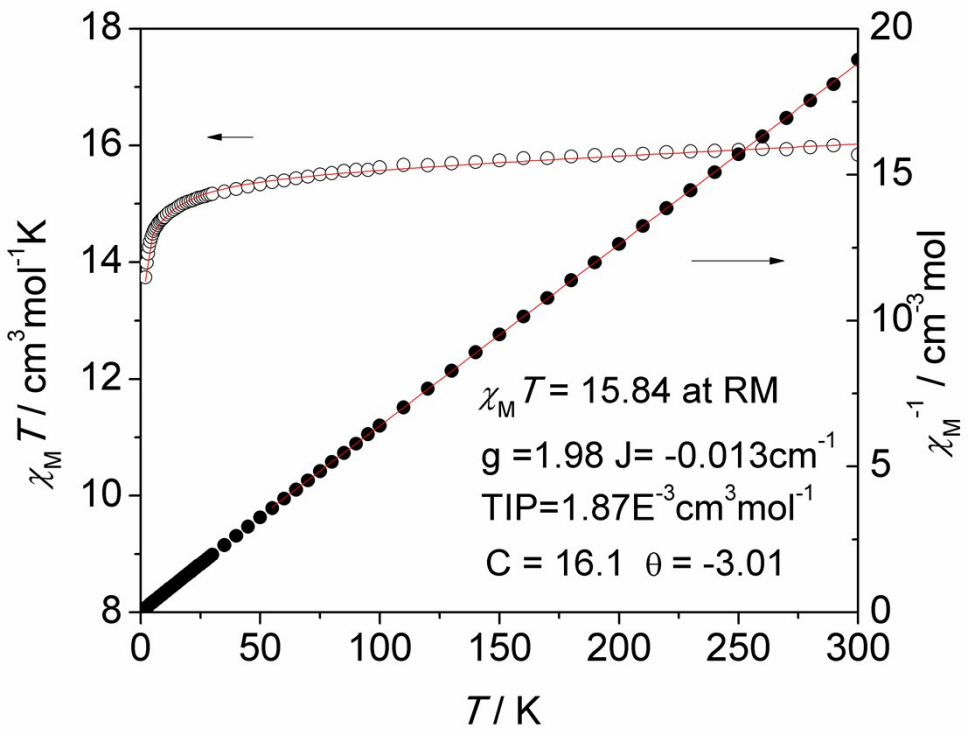

Fig. S12. Temperature dependence of the $\chi_M T$ versus T measured under 1000 Oe dc field for **6**. The solid line corresponds to the best fit for **6**.

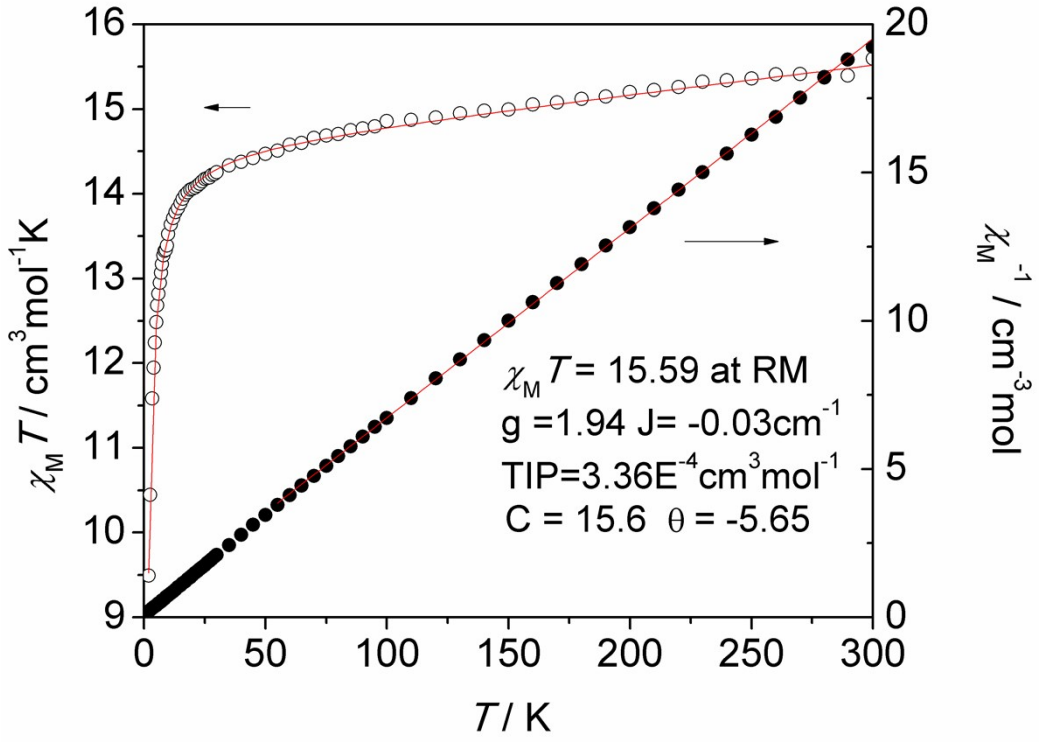

Fig. S13. Temperature dependence of the $\chi_M T$ versus T measured under 1000 Oe dc field for **7**. The solid line corresponds to the best fit for **7**.

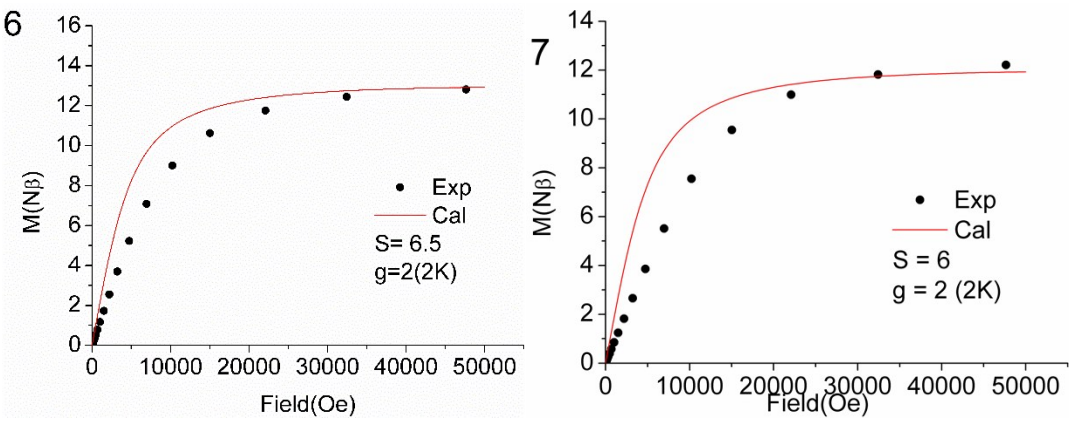

Fig. S14. Magnetization versus field data for **6** and **7** under 2K. [The red solid line is the Brillouin function for two magnetically isolated Gd(III) ions with g = 2.0]

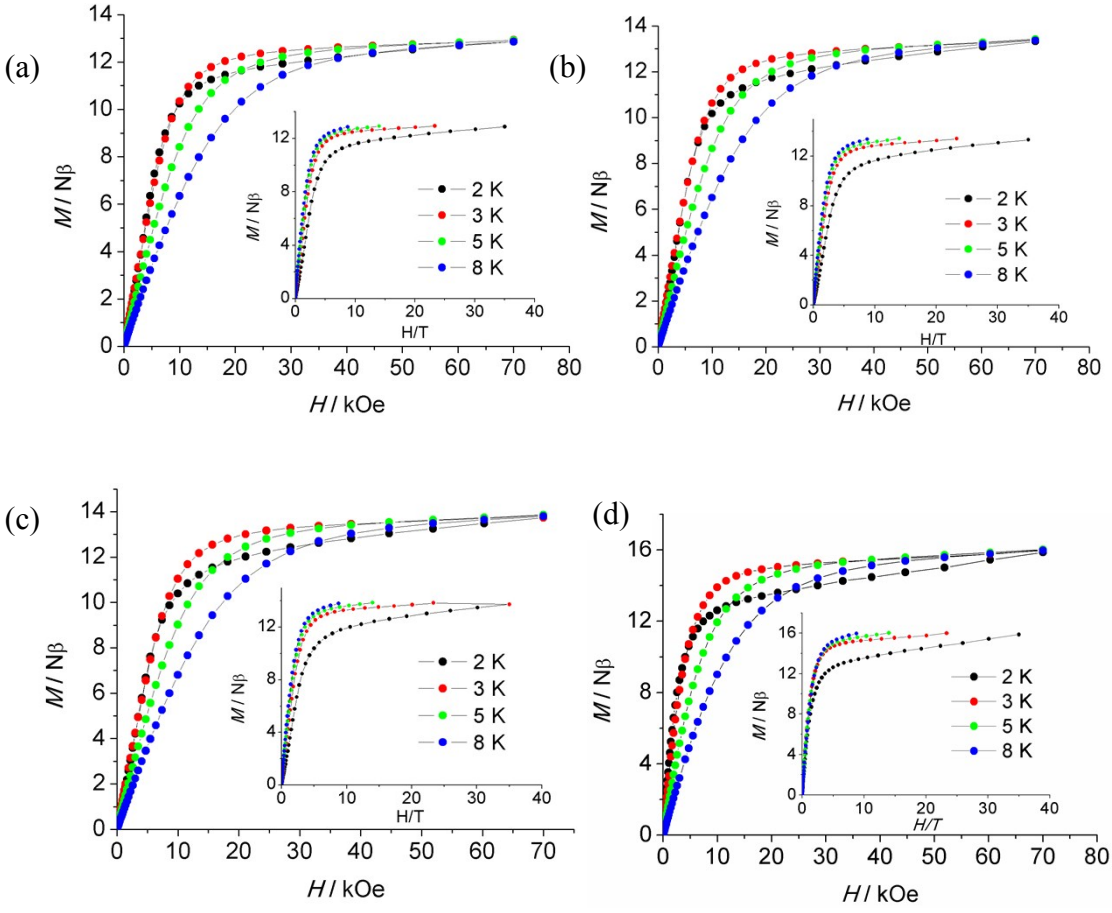

Fig. S15. Field dependences of magnetization in the field range 0-70 kOe and temperature range 2.0-8.0 K for **1**(a), **2**(b), **3**(c) and **1a**(d). Inset: Plots of the reduced magnetization *M* versus *H/T*.

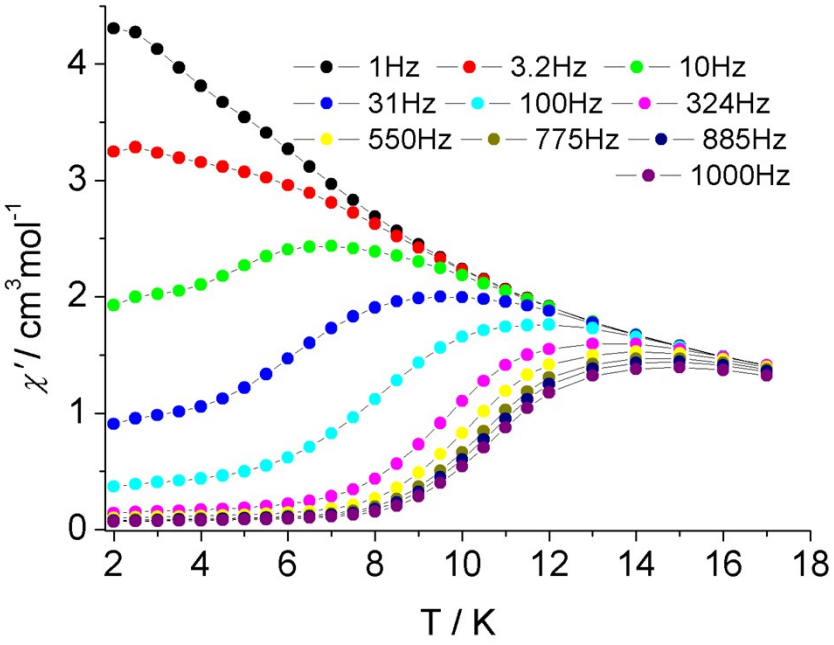

Fig. S16. Temperature dependence of the in-phase (χ') for complex **3** under zero dc field.

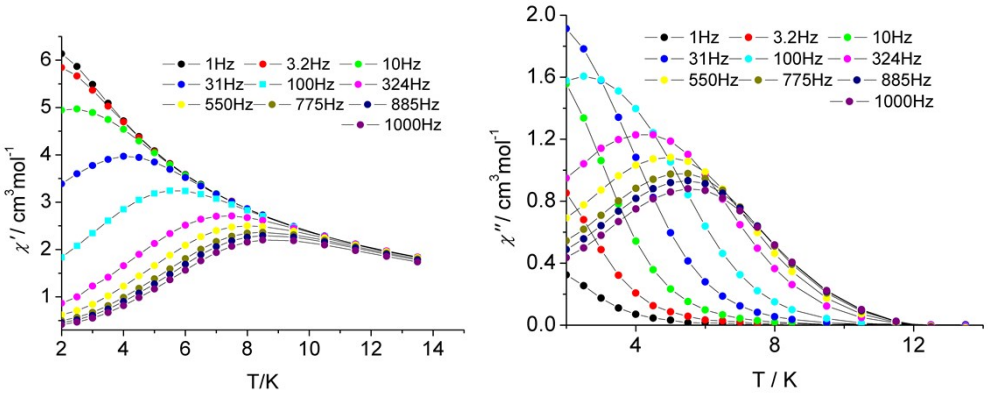

Fig. S17. Temperature dependence of the in-phase (χ') and out-of-phase (χ'') for complex **1** under zero dc field.

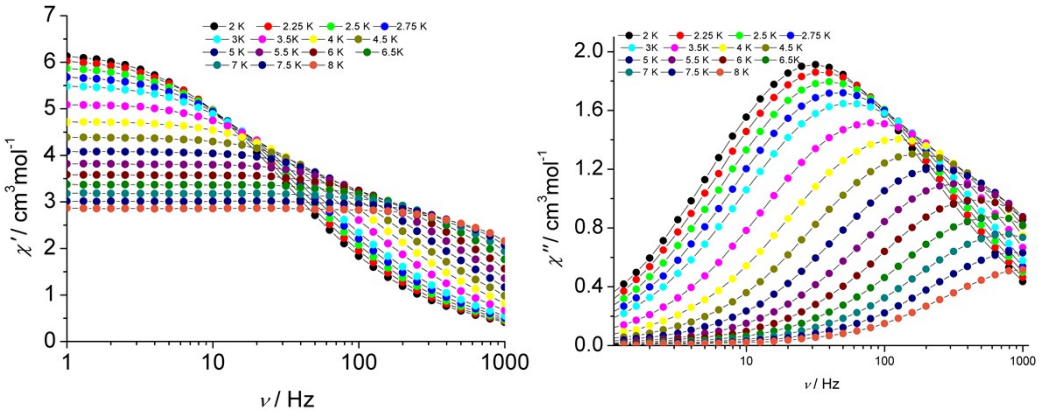

Fig. S18. Frequency dependence of the in-phase (χ') and out-of-phase (χ'') for complex **1** under zero dc field.

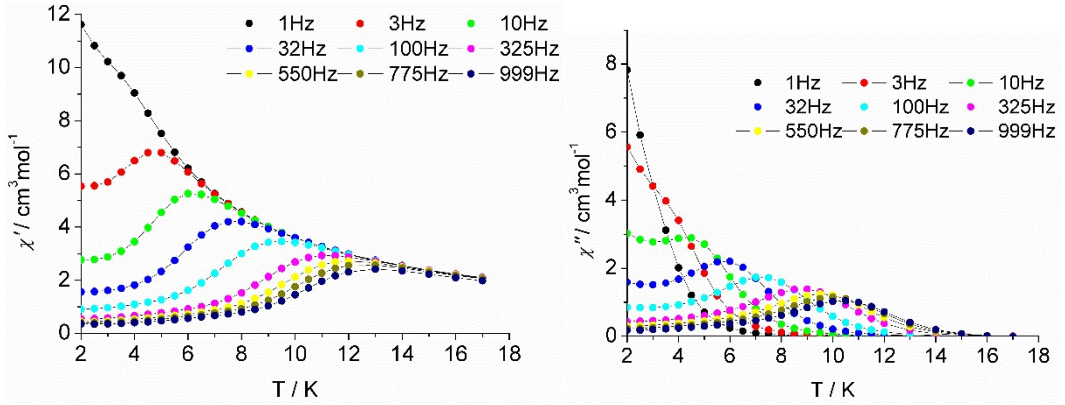

Fig. S19. Temperature dependence of the in-phase (χ') and out-of-phase (χ'') for complex **1a** under zero dc field.

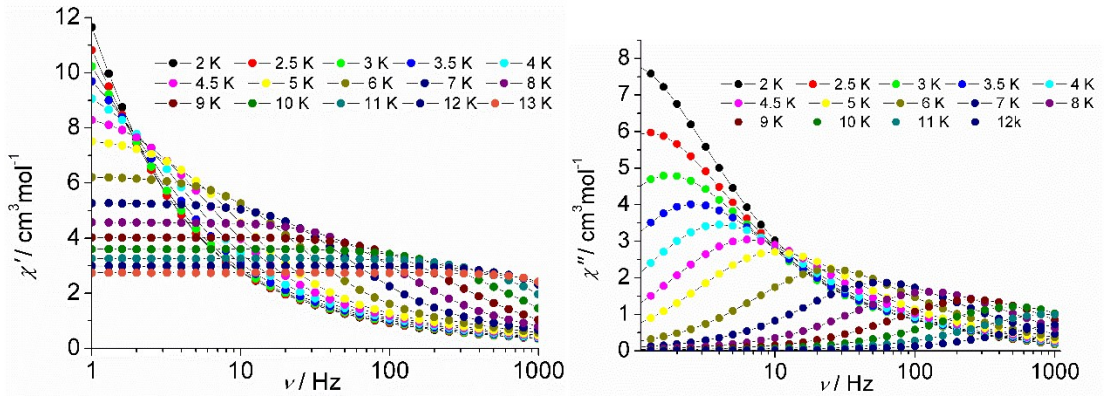

Fig. S20. Frequency dependence of the in-phase (χ') and out-of-phase (χ'') for complex **1a** under zero dc field.

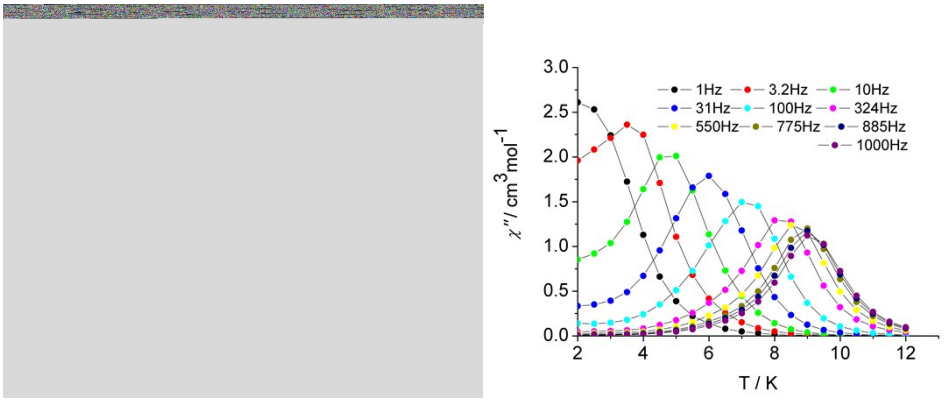

Fig. S21. Temperature dependence of the in-phase (χ') and out-of-phase (χ'') for complex **2** under zero dc field.

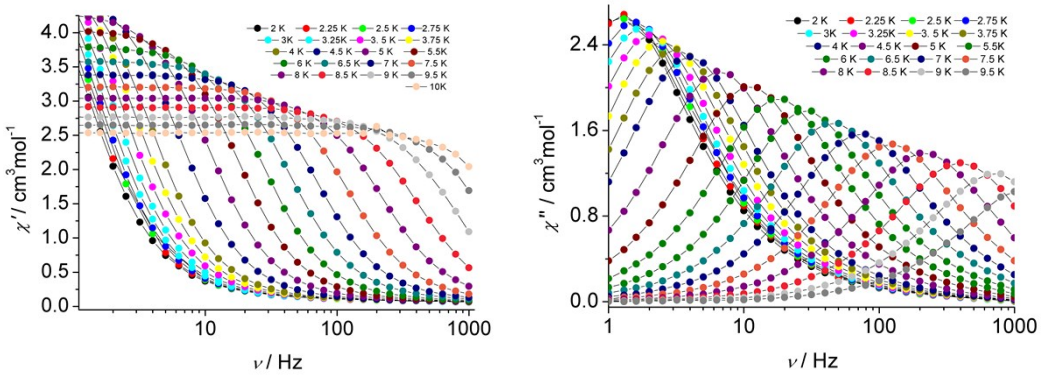

Fig. S22. Frequency dependence of the in-phase (χ') and out-of-phase (χ'') for complex **2** under zero dc field.

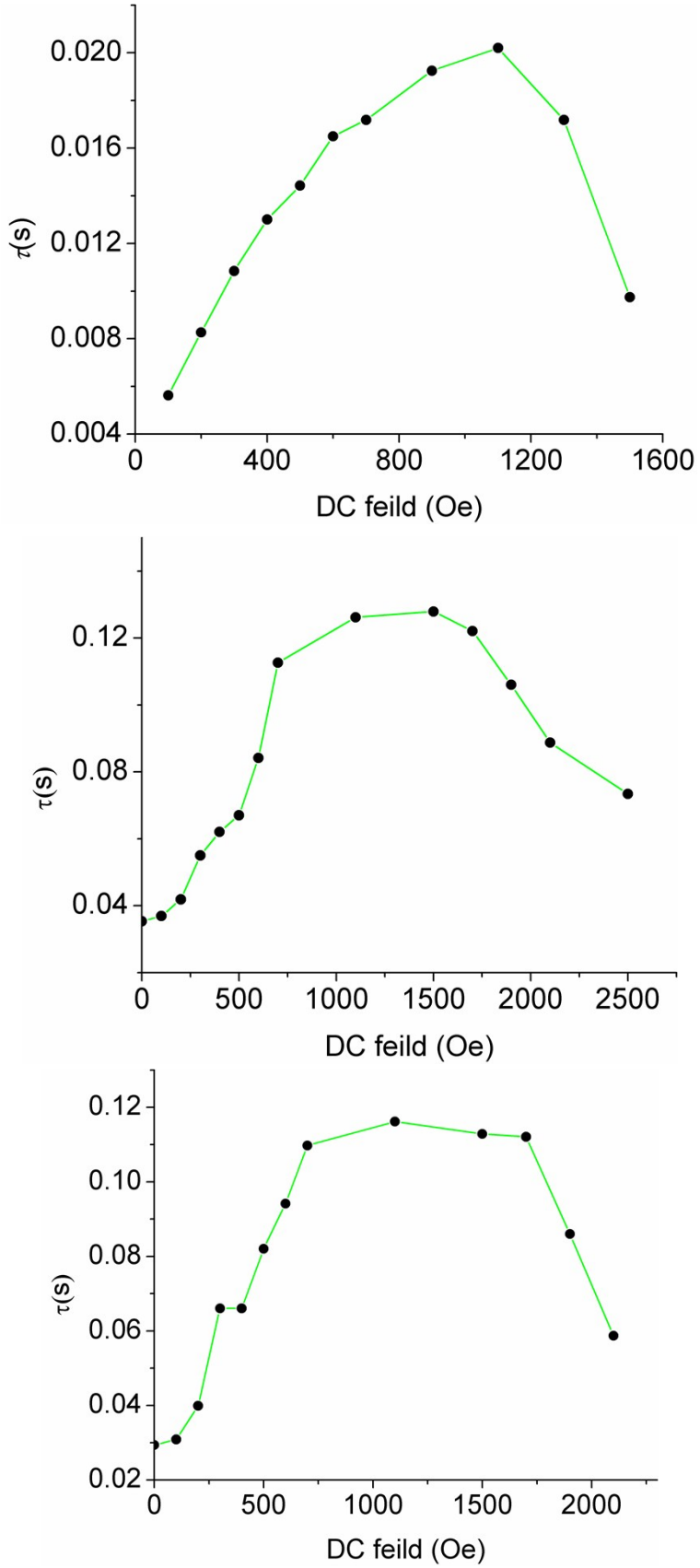

Fig. S23. Plot of τ vs. H for **1**(up), **2**(middle), **3**(bottom) under different dc fields at 2 K. The solid line is guide for eyes.

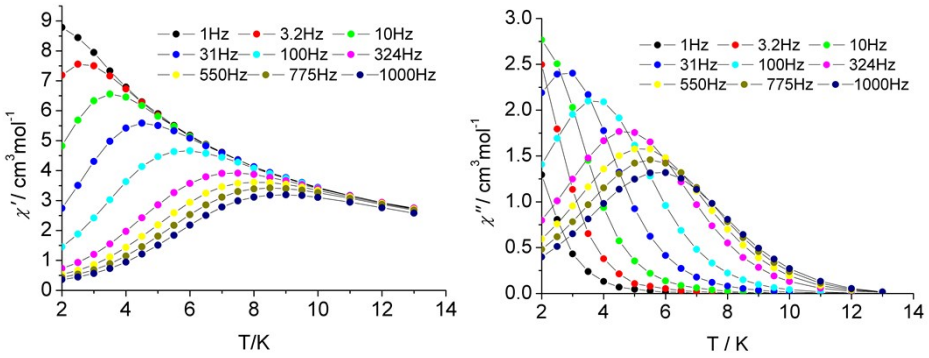

Fig. S24. Temperature dependence of the in-phase (χ') and out-of-phase (χ'') for complex **1** under 1100 Oe dc field.

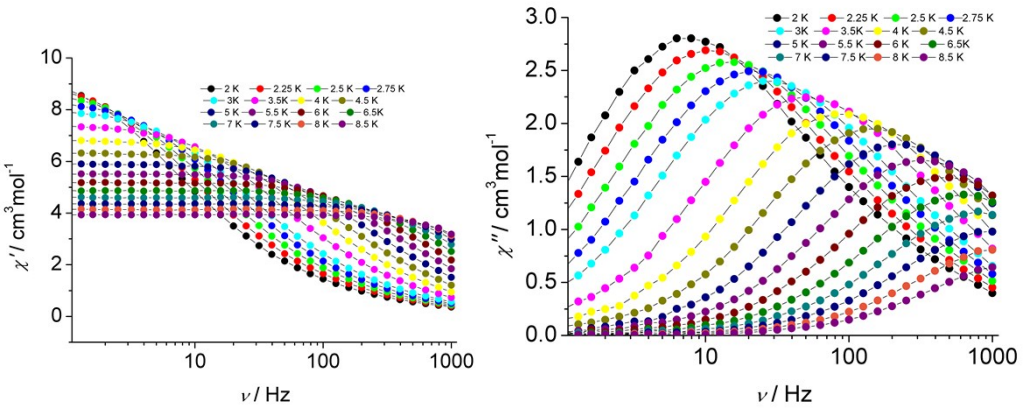

Fig. S25. Frequency dependence of the in-phase (χ') and out-of-phase (χ'') for complex **1** under 1100 Oe dc field.

Fig. S26. Temperature dependence of the in-phase (χ') and out-of-phase (χ'') for complex **1a** under 1500 Oe dc field.

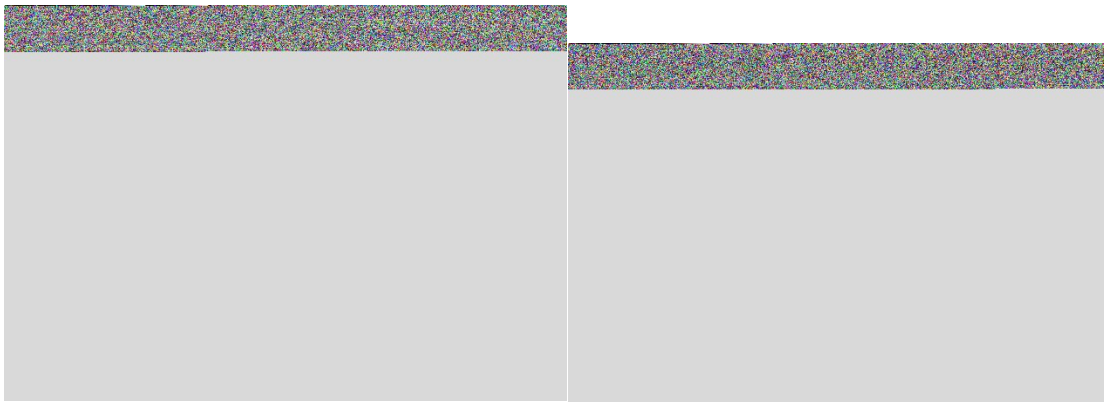

Fig. S27. Frequency dependence of the in-phase (χ') and out-of-phase (χ'') for complex **1a** under 1500 Oe dc field.

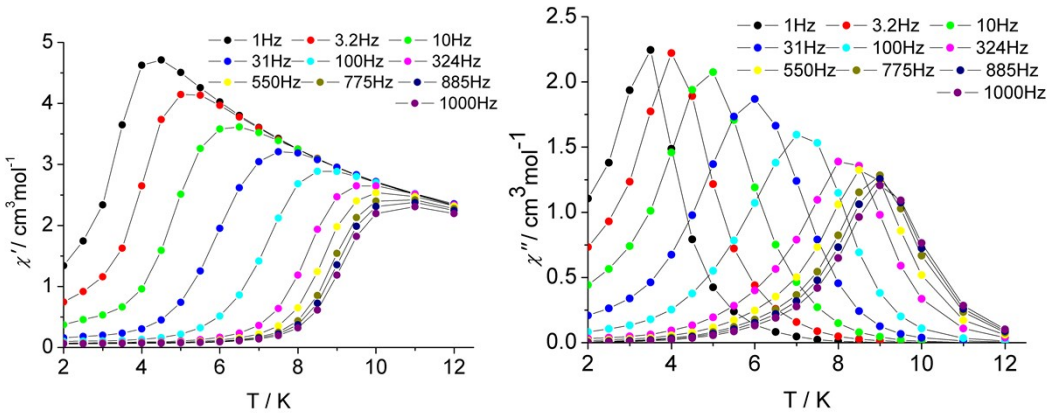

Fig. S28. Temperature dependence of the in-phase (χ') and out-of-phase (χ'') for complex **2** under 1500 Oe dc field.

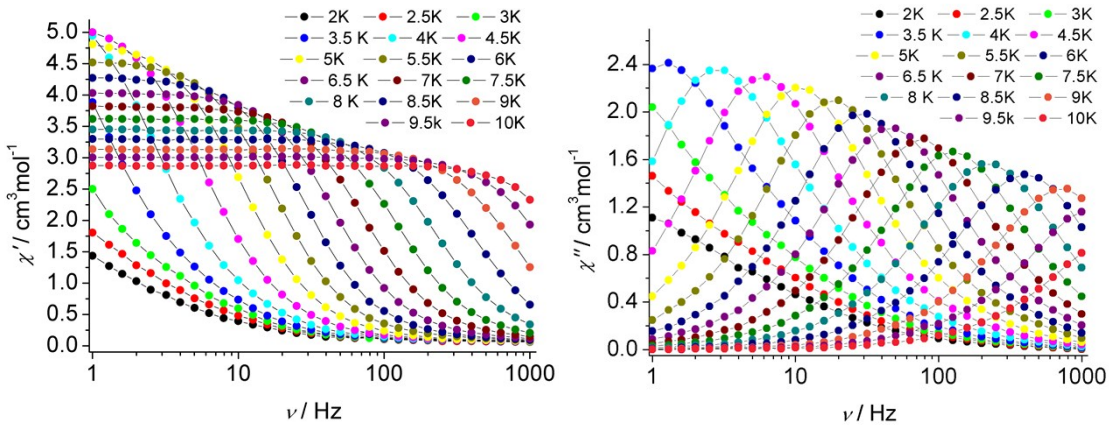

Fig. S29. Frequency dependence of the in-phase (χ') and out-of-phase (χ'') for complex **2** under 1500 Oe dc field.

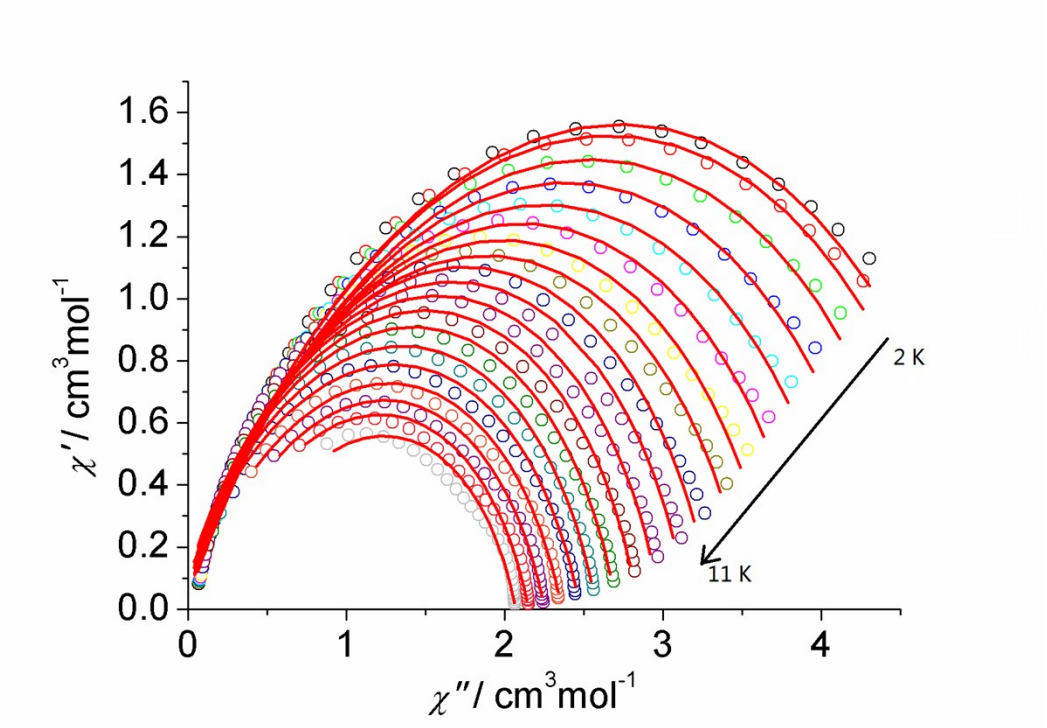

Fig. S30. The Cole-Cole plots of **3** in the temperature range of 2-11 K. The red lines are the best fits using an extended Debye model.

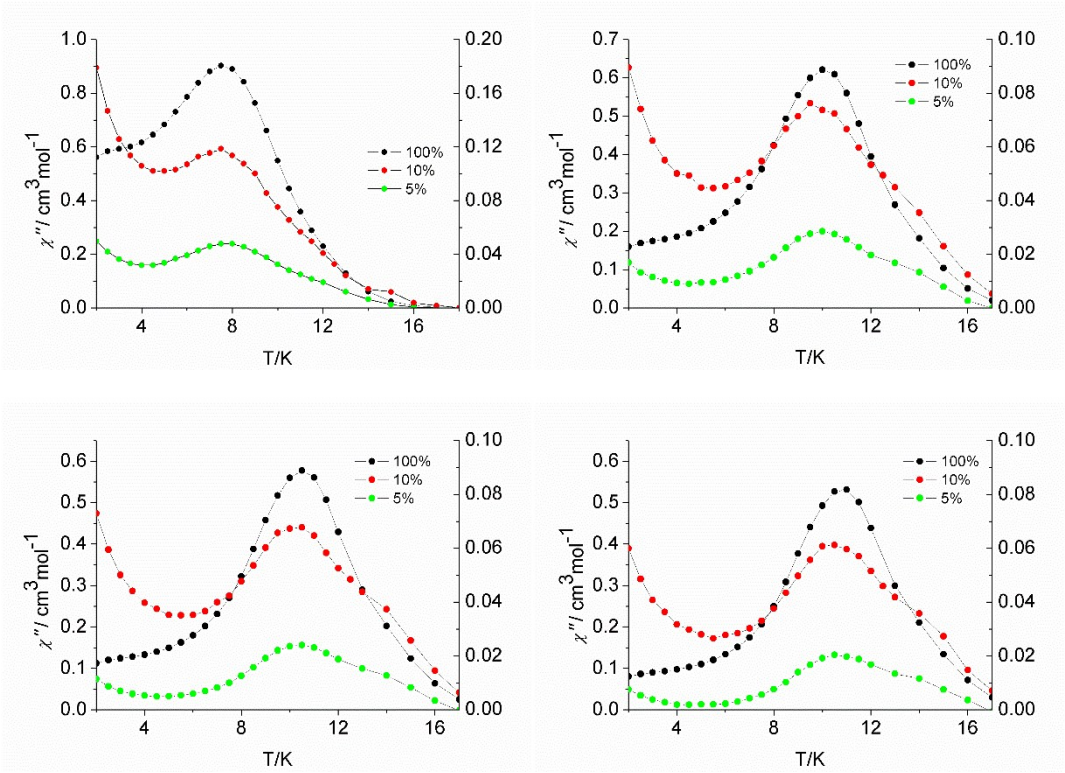

Fig. S31. Temperature dependence of the out-of-phase (χ'') plot at 100 Hz (top left), 550 Hz (top right), 775 Hz (bottom left), 1000 Hz (bottom right) under 0 dc field for the diluted samples.

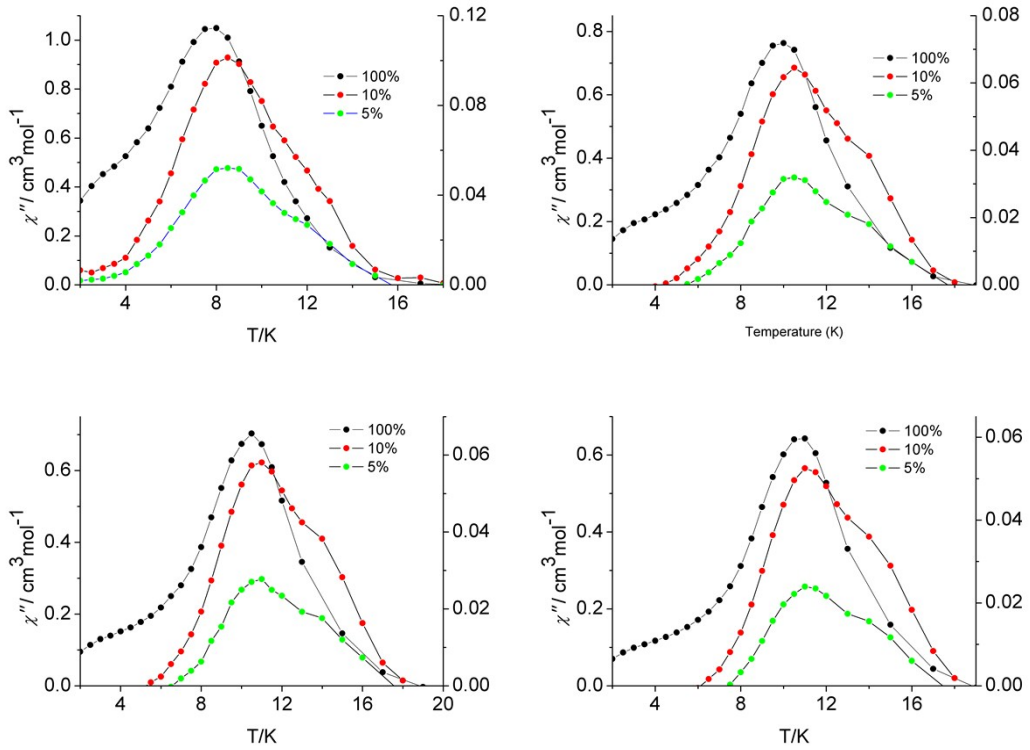

Fig. S32. Temperature dependence of the out-of-phase susceptibility (χ'') plot at 100 Hz (top left), 550 Hz (top right), 775 Hz (bottom left), 1000 Hz (bottom right) under 1500 Oe dc field for the diluted samples.

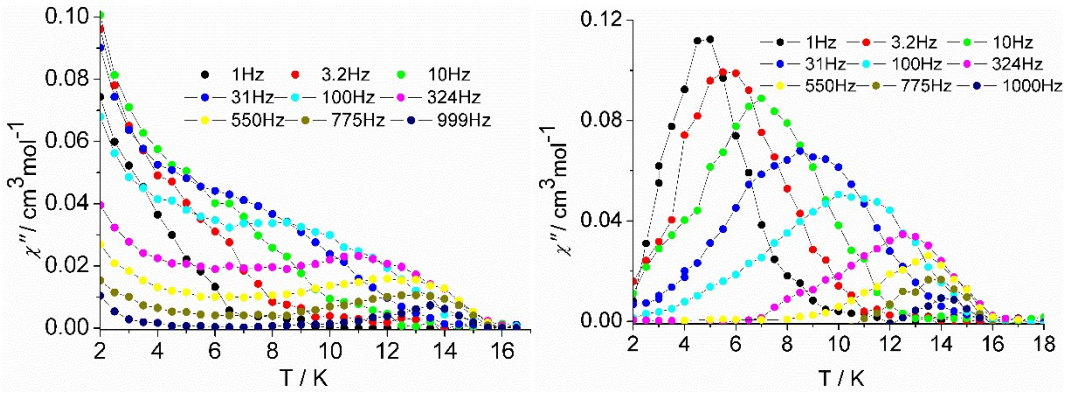

Fig. S33. Temperature dependence of out-of-phase (χ'') for **3M** under applied fields of 0 (left) and the 1500 Oe dc field (right).

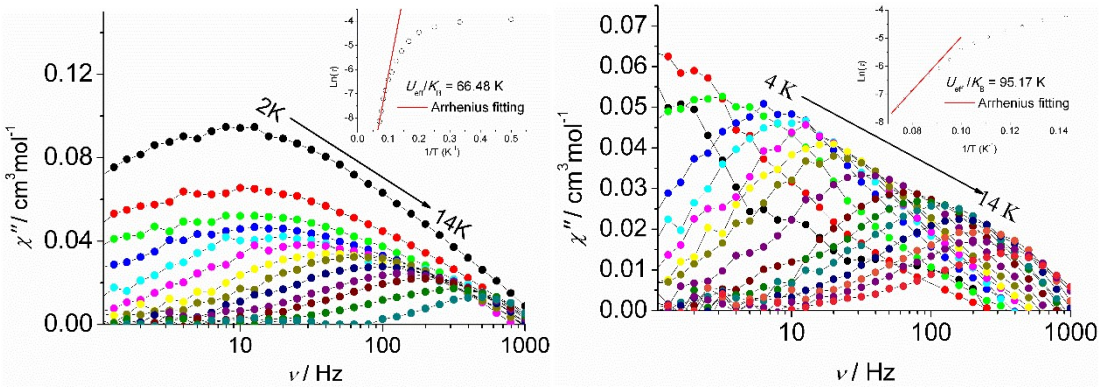

Fig. S34. Frequency dependence of out-of-phase (χ'') for **3M** under applied fields of zero (left) and 1500 Oe dc field (right). Inset: plot of ln(τ) vs. 1/T.

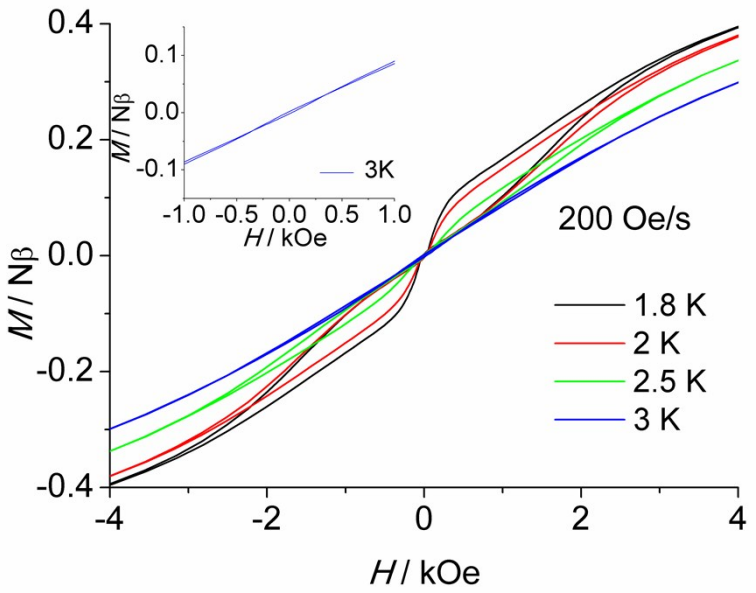

Fig. S35. Hysteresis loop for 10% Dy sample between 1.8 K and 3 K at the indicated sweep rates.

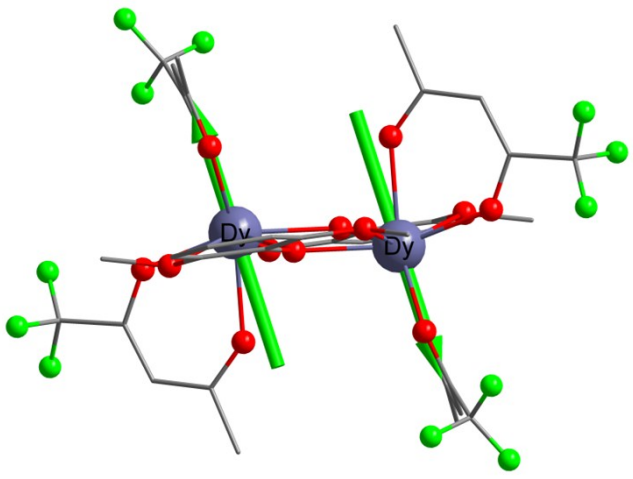

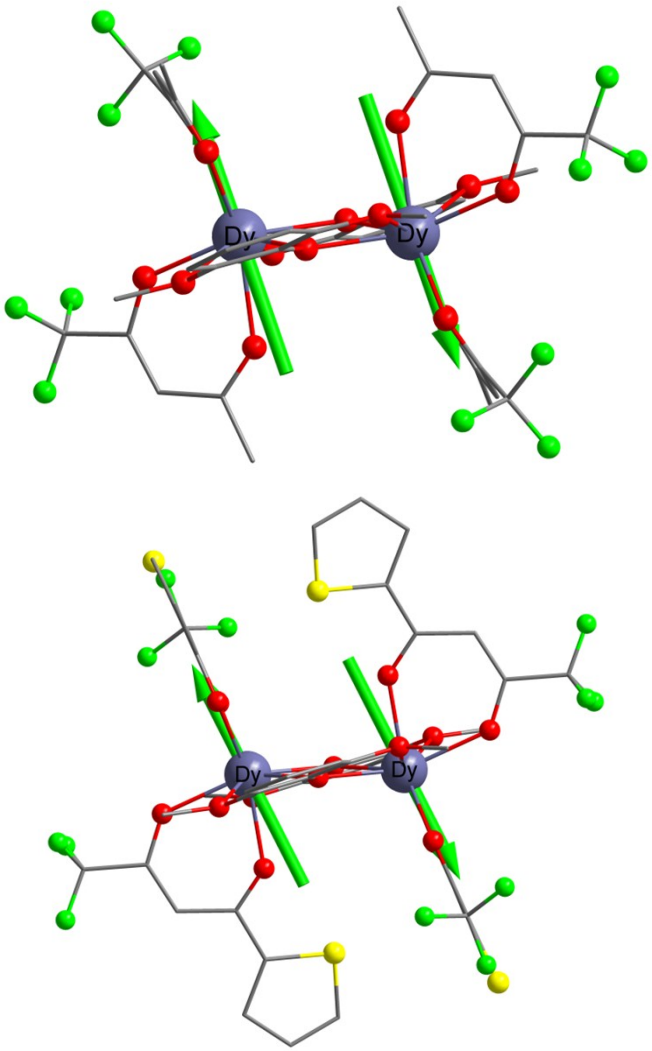

Fig. S36. Orientations of the local main magnetic axes of the ground doublets on Dy(III) ions of **1**(up), **2**(middle) and **3**(bottom).

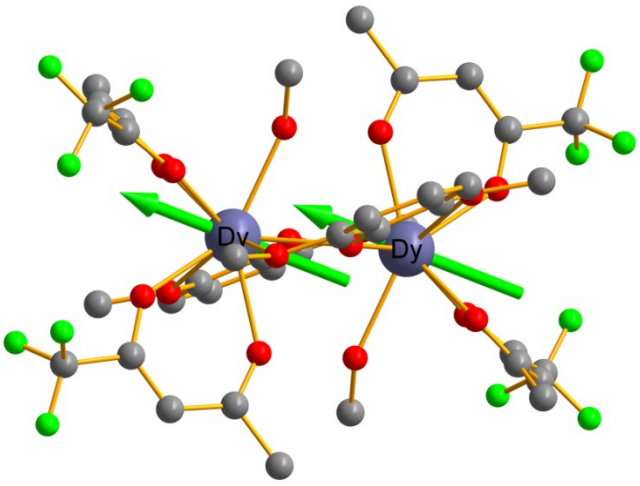

Fig. S37. Orientations of the local main magnetic axes of the ground doublets on Dy(III) ions of **1a**.

Computational details

There is only one type of Dy^{3+} ion for complex **1a**, and thus we need to calculate one Dy^{3+} fragment. There are two types of Dy^{3+} ions for each of complexes **1**–**3**, and thus we need to calculate two Dy^{3+} fragments for each of them. Complete-active-space self-consistent field (CASSCF) calculations on individual lanthanide Dy^{3+} fragment of the model structure extracted from each complex see Fig. S38 for the model structure) on the basis of X-ray determined geometry have been carried out with MOLCAS 7.8 program package.[S1]

During the calculations, the other three Dy^{3+} ions for each complex were replaced by diamagnetic Lu^{3+}. The basis sets for all atoms are atomic natural orbitals from the MOLCAS ANO-RCC library: ANO-RCC-VTZP for Dy^{3+} ions; VTZ for close O and N; VDZ for distant atoms. The calculations employed the second order Douglas-Kroll-Hess Hamiltonian, where scalar relativistic contractions were taken into account in the basis set and the spin-orbit couplings were handled separately in the restricted active space state interaction (RASSI-SO) procedure. For the fragment of Dy^{3+}, active electrons in 7 active spaces include all *f* electrons (CAS(9 in 7) in the CASSCF calculation. We have mixed the maximum number of spin-free state which was possible with our hardware (all from 21 sextets, 128 from 224 quadruplets, 130 from 490 doublets for the Dy^{3+} fragment).

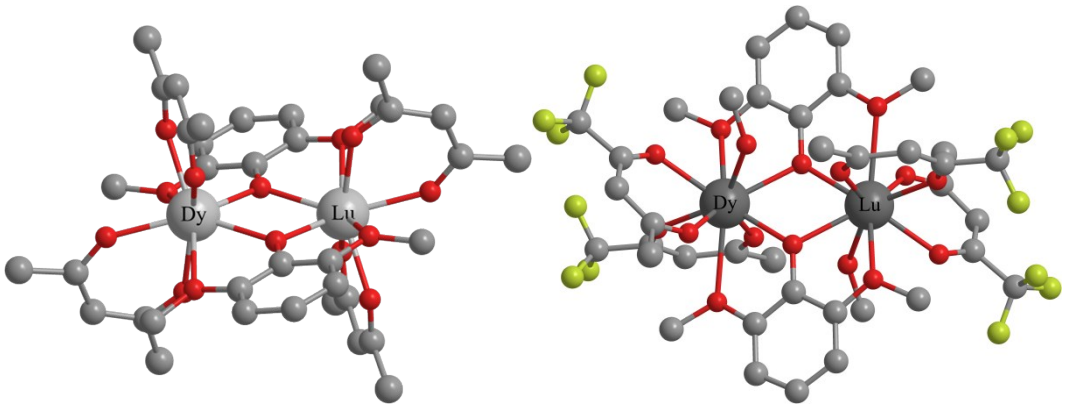

Fig. S38. Calculated model structure of complex **1** and **1a**. H atoms are omitted for clarity.

To fit the exchange interactions in four complexes, we took two steps to obtain them. Firstly, we calculated one Dy^{3+} fragment using CASSCF to obtain the corresponding magnetic properties. And then, the exchange interaction between the magnetic centers is considered within the Lines model,[S2] while the account of the dipole-dipole magnetic coupling is treated exactly. The Lines model is effective and has been successfully used widely in the research field of f-element single-molecule magnets.[S3]

For each of complexes **1**–**3**, there is only one type of *J*.

The exchange Hamiltonian is:

$$\hat{H}_{exch} = -J^{total}\,\hat{S}_{Dy1}\,\hat{S}_{Dy2}$$

The J^{total} is the parameter of the total magnetic interaction ($J^{total} = J^{diploar} + J^{exchange}$) between magnetic center ions. The $\hat{S}_{Dy} = \pm 1/2$ are the ground pseudospin on the Dy^{3+} sites. The dipolar magnetic coupling can be calculated exactly, while the exchange coupling constants were fitted through comparison of the computed and measured magnetic susceptibility and molar magnetization using the POLY_ANISO program.[S4]

Table S9. Energies (cm^{-1}) and ***g*** (g_x, g_y, g_z) tensors of the lowest spin-orbit states on one Dy^{3+} fragment of Dy-based complexes.

1		**2**		**3**		**1a**	
E	***g***	*E*	***g***	*E*	***g***	*E*	***g***
0.0	0.023 0.085 18.851	0.0	0.037 0.047 19.556	0.0	0.041 0.184 18.867	0.0	0.0297 0.0651 19.0179
30.1	0.024	45.3	0.014	39.3	0.082	101.2	0.0858

	0.109 18.447		0.067 19.264		0.119 18.644		0.1697 16.5708
134.5	0.295 0.419 13.971	138.5	0.222 0.528 14.177	147.3	0.356 0.512 15.266	188. 7	0.3476 0.4634 14.4674
172.2	5.238 5.913 8.048	193.8	8.284 6.129 3.782	197.3	1.527 2.012 9.274	229.4	1.6494 3.4311 13.4552
220.9	1.383 1.952 11.236	236.2	1.932 3.340 10.514	236.1	0.220 1.006 16.902	246.6	3.0649 5.0623 9.1534
311.5	0.055 1.036 13.765	321.5	0.103 0.761 13.880	251.7	4.485 6.266 9.155	295.9	1.4416 2.2017 12.0112
346.7	0.382 0.689 17.660	363.6	0.324 0.496 17.974	310.8	0.693 1.595 14.603	399.0	0.1553 0.2894 17.0576
474.2	0.033 0.059 19.229	487.3	0.032 0.055 19.299	443.6	0.033 0.089 19.051	591.1	0.0188 0.0270 19.5881

Table S10. Exchange energies (cm^{-1}) and main values of the g_z for the lowest two exchange doublets.

	1		**2**		**3**		**1a**	
	E	g_z	*E*	g_z	*E*	g_z	*E*	g_z
1	0.0	0.000	0.0	0.000	0.0	0.000	0.0	38.043

2	2.5	37.540	2.9	39.103	1.4	37.625	1.9	0.000

References:

S1 G. Karlstrom, R. Lindh, P. A. Malmqvist, B. O. Roos, U. Ryde, V. Veryazov, P. O. Widmark, M. Cossi, B. Schimmelpfennig, P. Neogrady and L. Seijo, MOLCAS: a Program Package for Computational Chemistry, *Comput. Mater. Sci.* 2003, **28**, 222.

S2 M. E. Lines, *J. Chem. Phys*., 1971, **55**, 2977.

S3 (a) K. C. Mondal, A. Sundt, Y. H. Lan, G. E. Kostakis, O. Waldmann, L. Ungur, L. F. Chibotaru, C. E. Anson and A. K. Powell, *Angew. Chem. Int. Ed*. 2012, **51**, 7550. (b) S. K. Langley, D. P. Wielechowski, V. Vieru, N. F. Chilton, B. Moubaraki, B. F. Abrahams, L. F. Chibotaru and K. S. Murray, *Angew. Chem. Int. Ed*., 2013, **52**, 12014.

S4 (a) L. F. Chibotaru, L. Ungur and A. Soncini, *Angew. Chem. Int. Ed.*, 2008, **47**, 4126. (b) L. Ungur, W. Van den Heuvel and L. F. Chibotaru, *New J. Chem.*, 2009, **33**, 1224. (c) L. F. Chibotaru, L. Ungur, C. Aronica, H. Elmoll, G. Pilet and D. Luneau, *J. Am. Chem. Soc.*, 2008, **130**, 12445.